

Rethinking the Importance of Sampling in Physics-informed Neural Networks

Arka Daw*
Virginia Tech
darka@vt.edu

Jie Bu*
Virginia Tech
jayroxis@vt.edu

Sifan Wang
University of Pennsylvania
sifanw@sas.upenn.edu

Paris Perdikaris
University of Pennsylvania
pgp@seas.upenn.edu

Anuj Karpatne
Virginia Tech
karpatne@vt.edu

Abstract

Physics-informed neural networks (PINNs) have emerged as a powerful tool for solving partial differential equations (PDEs) in a variety of domains. While previous research in PINNs has mainly focused on constructing and balancing loss functions during training to avoid poor minima, the effect of sampling collocation points on the performance of PINNs has largely been overlooked. In this work, we find that the performance of PINNs can vary significantly with different sampling strategies, and using a fixed set of collocation points can be quite detrimental to the convergence of PINNs to the correct solution. In particular, (1) we hypothesize that training of PINNs rely on successful “propagation” of solution from initial and/or boundary condition points to interior points, and PINNs with poor sampling strategies can get stuck at trivial solutions if there are *propagation failures*. (2) We demonstrate that propagation failures are characterized by highly imbalanced PDE residual fields where very high residuals are observed over very narrow regions. (3) To mitigate propagation failure, we propose a novel *evolutionary sampling* (Evo) method that can incrementally accumulate collocation points in regions of high PDE residuals. We further provide an extension of Evo to respect the principle of causality while solving time-dependent PDEs. We empirically demonstrate the efficacy and efficiency of our proposed methods in a variety of PDE problems.

1 Introduction

Our understanding of physical systems in a number of domains largely relies on our ability to solve partial differential equations (PDEs). While the conventional approach for solving PDEs is to use numerical methods such as finite elements methods (FEM)[19], a seminal line of work on using physics-informed neural networks (PINNs) [11] for solving PDEs has gained widespread attention [15, 18, 8, 1, 3, 4, 16]. The basic idea of PINNs for solving a forward PDE is to train a neural network to minimize errors w.r.t. the solution provided at initial/boundary points of a spatio-temporal domain, as well as the PDE residuals observed over a sample of interior points, referred to as collocation points. Despite the success of PINNs, it is known that PINNs can sometimes fail to converge to the correct solution in problems involving complicated PDEs, as reflected in several recent studies on characterizing the “failure modes” of PINNs [15, 18, 6]. Many of these failure modes are related to the susceptibility of PINNs in getting stuck at trivial solutions acting as poor local minima, due to the unique optimization challenges of PINNs. In particular, note that training PINNs is different from conventional ML problems as we only have access to the correct solution on the initial and/or

*These authors contributed equally to this work.

boundary points, while for all interior points in the domain, we can only compute PDE residuals. Also note that minimizing PDE residuals does not guarantee convergence to a correct solution since there are many trivial solutions of commonly observed PDEs that would show 0 residuals. While previous studies on understanding and preventing failure modes of PINNs have mainly focused on modifying network architectures or balancing loss functions during PINN training, the effect of sampling collocation points on avoiding failure modes of PINNs has been largely overlooked.

In this work, we present a novel perspective of failure modes of PINNs by postulating the propagation hypothesis: “in order for PINNs to avoid converging to trivial solutions at interior points, the correct solution must be *propagated* from the initial/boundary points to the interior points.” When this propagation is hindered, PINNs can get stuck at trivial solutions that are difficult to escape, referred to as the *propagation failure* mode. This hypothesis is motivated from a similar behavior observed in numerical methods where the solution of the PDE at initial/boundary points are iteratively propagated to interior points using finite differencing schemes [7].

We show that propagation failures in PINNs are characterized by highly imbalanced PDE residual fields, where very high residuals are observed in very narrow regions of the domain. Such high residual regions are not adequately sampled in the set of collocation points (which generally is kept fixed across all training iterations), making it difficult to overcome the propagation failure mode. This motivates us to develop sampling strategies that focus on selecting more collocation points from high PDE residual regions. This is related to the idea of local-adaptive mesh refinement used in FEM [19] to preferentially refine the computational mesh in regions with higher errors.

We propose a novel *evolutionary sampling* (Evo) strategy that can effectively accumulate collocation points in high PDE residual regions, thereby dynamically emphasizing on these skewed regions as we progress in training iterations. We also provide a causal extension of our proposed Evo algorithm (Causal Evo) that can explicitly encode the strong inductive bias of causality in propagation solution from initial points to interior points over training iterations, when solving time-dependent PDEs. We empirically demonstrate the efficacy and efficiency of our proposed sampling methods in a variety of PDE problems. We show the Evo and Causal Evo are able to mitigate propagation failure modes and converge to the correct solution with significantly smaller sample sizes and in lesser number of training iterations as compared to baseline methods, while incurring negligible computational overhead. We also demonstrate that simply performing dynamic random sampling at every epoch is a strong baseline that can achieve close to state-of-the-art performance on many benchmark PDEs, emphasizing the need to rethink the value of sampling in training PINNs.

2 Background and Related Work

Physics-Informed Neural Networks (PINNs). The basic formulation of PINN [10] for solving a forward PDE is to use a neural network $f_\theta(x, t)$ to infer the solution u of a general non-linear PDE:

$$u_t + \mathcal{N}_x[u] = 0, \quad x \in \mathcal{X}, t \in [0, T]; \quad u(x, 0) = h(x), \quad x \in \mathcal{X}; \quad u(x, t) = g(x, t), \quad t \in [0, T], x \in \partial\mathcal{X}$$

where x and t are the space and time coordinates respectively, \mathcal{X} is the spatial domain, $\partial\mathcal{X}$ is the boundary of spatial domain, and T is the time horizon. The PDE is enforced on the entire spatio-temporal domain ($\Omega = \mathcal{X} \times [0, T]$) on a set of collocation points $\{\mathbf{x}_r^i = (x_r^i, t_r^i)\}_{i=1}^{N_r}$ by computing the PDE residual ($\mathcal{R}(x, t)$) and the corresponding PDE Loss (\mathcal{L}_r) as follows:

$$\mathcal{R}_\theta(x, t) = \frac{\partial}{\partial t} f_\theta(x, t) - \mathcal{N}_x[f_\theta(x, t)] \quad (1)$$

$$\mathcal{L}_r(\theta) = \mathbb{E}_{\mathbf{x}_r \sim p(\Omega)}[\mathcal{R}_\theta(\mathbf{x}_r)^2] \approx \frac{1}{N_r} \sum_{i=1}^{N_r} [\mathcal{R}_\theta(x_r^i, t_r^i)]^2 \quad (2)$$

where the PDE Loss is defined as the expectation of the squared PDE Residuals approximated using a set of collocation points sampled from a uniform probability distribution p . PINNs approximate the solution of the PDE by optimizing the following overall loss function $\mathcal{L} = \lambda_r \mathcal{L}_r(\theta) + \lambda_{bc} \mathcal{L}_{bc}(\theta) + \lambda_{ic} \mathcal{L}_{ic}(\theta)$, where \mathcal{L}_r is the PDE loss, \mathcal{L}_{ic} and \mathcal{L}_{bc} are the mean squared loss on the initial and boundary data respectively, and $\lambda_r, \lambda_{ic}, \lambda_{bc}$ are the set of hyperparameters that control the interplay between the different loss terms. Although PINNs can be applied to inverse problems, i.e., estimate PDE parameters from observed data, we only focus on forward problems in this paper.

Prior Work on Characterizing Failure Modes of PINNs. Despite the popularity of PINNs in approximating PDEs, several work have emphasized the presence of failure modes while training

PINNs. One early work [15] demonstrated that imbalance in the gradients of multiple loss terms could lead to poor convergence of PINNs, motivating the development of Adaptive PINNs. Another recent development [18] made use of the Neural Tangent Kernel (NTK) theory to indicate that the different convergence rates of the loss terms can lead to training instabilities. Large values of PDE coefficients have also been connected to possible failure modes in PINNs [6]. In all these works, the effect of sampling to characterize and mitigate these failure modes has been largely overlooked. Although a recent work has demonstrated the use of Importance Sampling [9] to improve the convergence speed of PINNs, the proposed method uses a very large pool of collocation points to approximate the PDE residuals, making such a sampling approach difficult to scale up for complex PDEs. Another recent development named Causal PINNs [17] demonstrated that the principle of causality can be violated while training PINNs for time-dependent PDEs and proposed an explicit way of incorporating the causal structure in the training procedure. However, this solution can only be applied to time-dependent PDEs, and as we demonstrate empirically in Section 5, also requires large sample sizes.

3 Propagation Hypothesis: A New Perspective of Failure Modes in PINNs

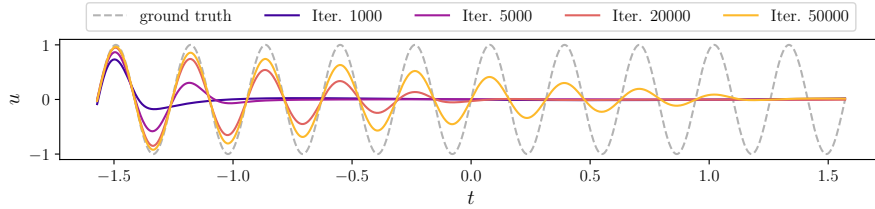


Figure 1: PINN solutions for a simple ODE: $u_{xx} + k^2 u = 0$ ($k = 20$) with the analytical solution, $u = A \sin(kx) + B \cos(kx)$. We can see smooth *propagation* of the correct solution from the boundary point at $x = 0$ to interior points ($x > 0$) as we increase training iterations.

What is Unique About Training PINNs? Training PINNs presents fundamentally different optimization challenges than those encountered in conventional ML problems. In a conventional supervised ML problem, the correct solution for the training sample are known and are considered representative of the test samples such that the trained ML model can easily be extrapolated on closely situated test samples. However, in the context of PINNs, we only have access to the “correct” solution of the PDE on the initial and/or boundary points, while not having any labels for the interior points in the spatio-temporal domain Ω . Note that the interior points in Ω can be quite far away from the initial/boundary points, making extrapolation difficult. Further, training PINNs involves minimizing the PDE residuals over a set of collocation points sampled from Ω . However, minimizing PDE residuals alone is not sufficient to ensure convergence to the correct solution, since there may exist many trivial solutions of a PDE showing very small residuals. For example, $u(x, t) = 0$ is a trivial solution for any homogeneous PDE, which a neural network is likely to get stuck at in the absence of correct solution at initial/boundary points. Another unique aspect of training PINNs is that minimizing PDE residuals requires computing the gradients of the output w.r.t. (x, t) (e.g., u_x and u_t). Hence, the solution at a collocation point is affected by the solutions at nearby points leading to local propagation of solutions.

Propagation Hypothesis. In light of the unique properties of PINNs, we postulate that in order for PINNs to converge to the “correct” solution, the correct solution must propagate from the initial and/or boundary points to the interior points as we progress in training iterations. We draw inspiration for this hypothesis from a similar behavior observed in numerical methods for solving PDEs, where the solution of the PDE at initial/boundary points are iteratively propagated to interior points using finite differencing schemes [7]. Figure 1 demonstrates the propagation hypothesis of PINNs for a simple ordinary differential equation (ODE).

Propagation Failure: Why It Happens and How to Diagnose? As a corollary of the propagation hypothesis, PINNs can fail to converge to the correct solution if the solution at initial/boundary points is *unable to propagate* to interior points during the training process. We call this phenomenon the “*propagation failure*” mode of PINNs. This is likely to happen if some collocation points start converging to trivial solutions before the correct solution from initial/boundary points is able to reach them. Such collocation points would also propagate their trivial solutions to nearby interior points, leading to a cascading effect in the learning of trivial solutions over large regions of Ω and further hindering the propagation of the correct solution from initial/boundary points.

To *diagnose* propagation failures, note that the PDE residuals are expected to be low over both types of regions: regions that have converged to the correct solution and regions that have converged to trivial solutions. However, the boundaries of these two types of regions would show a sharp discontinuity in solutions, leading to very high PDE residuals in very narrow regions. A similar phenomenon is observed in numerical methods where sharp high-error regions disrupt the evolution of the PDE solution at surrounding regions, leading to cascading of errors. We use the imbalance of high PDE residual regions as a diagnosis tool for characterizing propagation failure modes in PINNs.

To demonstrate propagation failure, let us consider an example PDE for the convection equation: $\frac{\partial u}{\partial t} + \beta \frac{\partial u}{\partial x} = 0$, $u(x, 0) = h(x)$, where β is the convection coefficient and $h(x)$ is the initial condition (see Appendix for details about this PDE). In a previous work [6], it has been shown that PINNs fail to converge for this PDE for $\beta > 10$. We experiment with two cases, $\beta = 10$ and $\beta = 50$, in Figure 2. We can see that the PDE residual loss steadily decreases with training iterations for both these cases, but the relative error w.r.t. the ground-truth solution only decreases for $\beta = 10$, while for $\beta = 50$, it remains flat. This suggests that for $\beta = 50$, PINN is likely getting stuck at a trivial solution that shows low PDE residuals but high errors. To diagnose this failure mode, we plot two additional metrics in Figure 2 to check for the imbalance in high PDE residual regions: Fisher-Pearson’s coefficient of Skewness [5] and Fisher’s Kurtosis [5] (see Appendix for computation details). High Skewness indicates lack of symmetry in the distribution of PDE residuals while high Kurtosis indicates the presence of a heavy-tail. For $\beta = 10$, we can see that both Skewness and Kurtosis are relatively small across all iterations, indicating absence of imbalance in the high residual regions. However, for $\beta = 50$, both these metrics shoot up significantly as the training progresses, which indicates the formation of very high residuals in very narrow regions—a characteristic feature of the propagation failure mode. Figure 3 confirms that this indeed is the case by visualizing the PINN solution and PDE residual maps. We see similar trends of propagation failure for other values of $\beta > 10$ (see Appendix).

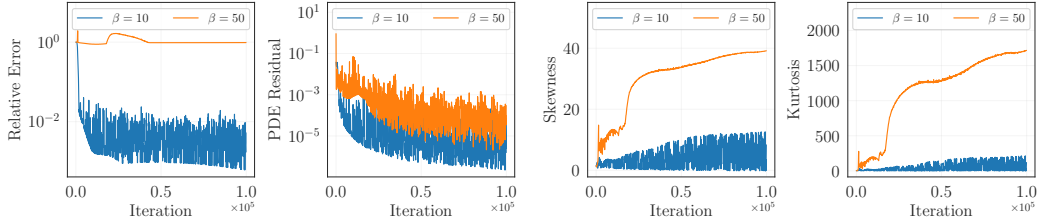


Figure 2: Demonstration of propagation failure while solving the convection equation with $\beta = 50$.

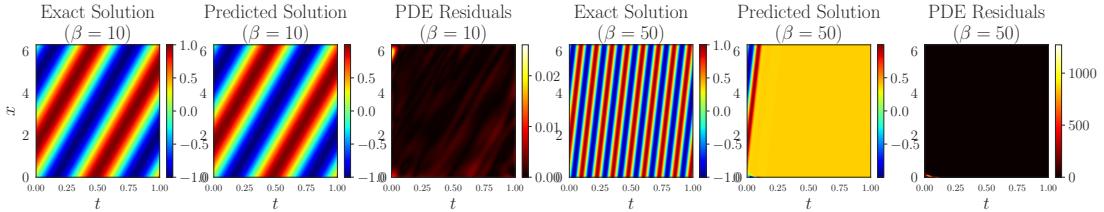


Figure 3: Demonstration of the Exact PDE solution, the predicted PDE solution, and the PDE Residual Field for the convection equation with $\beta = 10$ and $\beta = 50$ respectively.

4 Mitigating Propagation Failures in PINNs: Proposed Approaches

Rationale for Proposed Sampling Schemes. Since *propagation failure* in PINNs is characterized by very high PDE residuals appearing in very narrow regions, we consider the objective of sampling more collocation points from high residual regions at every training iteration to avoid propagation failure. The rationale for this objective is that if we can adequately represent high residual regions in the training process, we can break the propagation barrier regions with high residuals appearing at the boundaries of correct and trivial solutions, and thus enable the solution at initial/boundary points to easily propagate to the interior points. In particular, at every training iteration, we consider the goal of sampling a collocation point $\mathbf{x}_r \in \Omega$ with probability proportional to the absolute value of the PDE residual at \mathbf{x}_r , i.e., $p(\mathbf{x}_r) \propto |\mathcal{R}(\mathbf{x}_r)|$. This sampling objective is motivated by a related strategy of *local-adaptive mesh refinement* developed for Finite Element Methods (FEM) [19], where

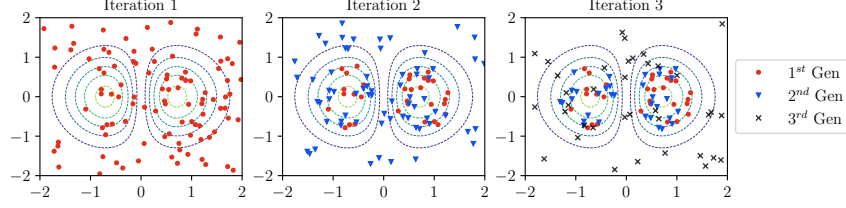


Figure 4: Schematic to describe our proposed evolutionary sampling algorithm, where collocation points are incrementally accumulated in regions with high PDE residuals (shown as contour lines).

the goal is to preferentially refine the computational mesh used in numerical methods based on the localization of the errors. It is also related to the idea of *boosting* in ensemble learning where training samples with larger errors at a certain epoch are assigned higher weights of being picked in the next epoch, to increasingly focus on high error regions [12].

There are two primary challenges in implementing a sampling strategy where collocation points are selected based on their absolute PDE residuals. *First*, at every training iteration, we are only able to observe the PDE residuals over a fixed set of N_r collocation points. This makes it difficult to estimate the value of the PDE residual over any arbitrary point $\mathbf{x}_r \in \Omega$, especially when N_r is kept small to reduce training costs or in high-dimensional domains where sampling is expensive. *Second*, the PDE residual at any point \mathbf{x}_r keeps dynamically changing over the training process, necessitating the sampling strategy to be run at frequent iterations. This makes it impractical to use computationally expensive sampling strategies such as Rejection Sampling or Monte Carlo-based Sampling [13].

Dynamic Random Sampling: A Strong Baseline. A very simple baseline for mitigating propagation failure is to *dynamically* sample a random set of N_r collocation points at every iteration, independently of previous iterations. To see how this simple sampling strategy can help in sampling points from high PDE residual regions, let us consider partitioning the entire input domain Ω into two subsets: regions with high PDE residuals, Ω_{high} , and regions with low PDE residuals Ω_{low} . If the high PDE residual regions are imbalanced because of propagation failure, we would expect that the area of Ω_{high} (A_{high}) is significantly smaller than the area of Ω_{low} (A_{low}), i.e., $A_{high} \ll A_{low}$. Let us compute the probability of sampling at least one collocation point from Ω_{high} across all epochs of PINN training. If we use a *fixed* set of collocation points sampled from a uniform distribution at every epoch, this probability will be equal to $A_{high}/(A_{high} + A_{low})$, which can be very small. Hence, we are likely to under-represent points from Ω_{high} in the training process and thus get stuck in trivial solutions with high residual regions around its boundaries, especially when N_r is low.

On the other hand, if we perform *dynamic* sampling, the probability of picking at least one point from Ω_{high} across all epochs will be equal to $1 - (1 - A_{high}/(A_{high} + A_{low}))^K$, where K is the number of epochs. We can see that when K is large, this probability approaches 1, indicating that across all epochs of PINN training, we would have likely sampled a point from Ω_{high} in at least one epoch, and used it to minimize its PDE residual. As we empirically demonstrate later in Section 5, dynamic sampling is indeed able to control the skewness of PDE residuals compared to fixed sampling, and thus act as a strong baseline for mitigating propagation failures.

However, note that even if we use dynamic sampling, the contribution of points from Ω_{high} in the overall PDE residual loss computed at any epoch is still low. In particular, since the probability of sampling points from Ω_{high} at any epoch is equal to $A_{high}/(A_{high} + A_{low})$, the expected PDE residual loss computed over all collocation points will be equal to

$$\mathbb{E}_{\Omega}[\mathcal{L}_r(\theta)] = \mathbb{E}_{\Omega_{high}}[\mathcal{L}_r(\theta)] \times \frac{A_{high}}{A_{high} + A_{low}} + \mathbb{E}_{\Omega_{low}}[\mathcal{L}_r(\theta)] \times \frac{A_{low}}{A_{high} + A_{low}} \quad (3)$$

Since $A_{high} \ll A_{low}$, the gradient update of θ at every epoch will be dominated by the low PDE residuals observed over points from Ω_{low} , leading to slow propagation of information from initial/boundary points to interior points.

4.1 Evolutionary Sampling (Evo)

To motivate our proposed sampling strategy, we ask the question: “How can we make our collocation points evolve over iterations such that they start accumulating in regions with high PDE residuals of

Algorithm 1 Proposed Evolutionary Sampling Algorithm For PINN

- 1: Sample the initial population \mathcal{P}_0 of N_r collocation points $\mathcal{P}_0 \leftarrow \{\mathbf{x}_r\}_{i=1}^{N_r}$ from a uniform distribution $\mathbf{x}_r^i \sim \mathcal{U}(\Omega)$, where Ω is the input domain ($\Omega = [0, T] \times \mathcal{X}$).
 - 2: **for** $i = 0$ to $\text{max_iterations} - 1$ **do**
 - 3: Compute the fitness of collocation points $\mathbf{x}_r \in \mathcal{P}_i$ as $\mathcal{F}(\mathbf{x}_r) = |\mathcal{R}(\mathbf{x}_r)|$.
 - 4: Compute the threshold $\tau_i = \frac{1}{N_r} \sum_{j=1}^{N_r} \mathcal{F}(\mathbf{x}_r^j)$
 - 5: Select the retained population \mathcal{P}_i^r such that $\mathcal{P}_i^r \leftarrow \{\mathbf{x}_r^j : \mathcal{F}(\mathbf{x}_r^j) > \tau_i\}$
 - 6: Generate the re-sampled population $\mathcal{P}_i^s \leftarrow \{\mathbf{x}_r^j : \mathbf{x}_r^j \sim \mathcal{U}(\Omega)\}$
 - 7: Merge the two populations $\mathcal{P}_{i+1} \leftarrow \mathcal{P}_i^r \cup \mathcal{P}_i^s$
 - 8: **end for**
-

every iteration?” Inspired by algorithms used for modeling biological evolution [2], we present a novel sampling strategy termed *Evolutionary Sampling (Evo)*, where the population of collocation points is dynamically evolved at every iteration by retaining points with high PDE residuals from the current population and re-sampling new points from a uniform distribution. As shown in Figure 4, Evo incrementally accumulates collocation points from high PDE residual regions as training iterations progress, thus ensuring their adequate representation in the optimization process.

Analogous to evolutionary algorithms developed in optimization literature [14], we introduce a notion of “fitness” for every collocation point such that points with higher fitness are allowed to survive in the next iteration, mimicking the “survival of fittest” philosophy. In particular, we define the fitness of a collocation point $\mathbf{x}_r \in \Omega$ as the absolute value of its PDE residual, i.e., $\mathcal{F}(\mathbf{x}_r) = |\mathcal{R}(\mathbf{x}_r)|$. At iteration 0, we start the sampling process using an initial population \mathcal{P}_0 of N_r collocation points generated from a uniform distribution. To sample points at the next iteration, we *retain* collocation points in \mathcal{P}_0 whose fitness value is greater than a threshold relative to other points in \mathcal{P}_0 , and *re-sample* the remainder points from a uniform distribution. More formally, at iteration i , we construct the “retained population” \mathcal{P}_i^r comprising of points from \mathcal{P}_i with high fitness values as follows: $\mathcal{P}_i^r \leftarrow \{\mathbf{x}_r^j : \mathcal{F}(\mathbf{x}_r^j) > \tau_i\}$, where τ_i is the relative threshold at iteration i . In our experiments, we set τ_i equal to the expectation of fitness values over all points in \mathcal{P}_i . The remainder of collocation points are re-sampled from a uniform distribution which constitutes the “re-sampled population” \mathcal{P}_i^s , i.e., $\mathcal{P}_i^s \leftarrow \{\mathbf{x}_r^j : \mathbf{x}_r^j \sim \mathcal{U}(\Omega)\}$. The retained population and the re-sampled population are then merged to generate the population for the next iteration \mathcal{P}_{i+1} .

Algorithm 1 shows the pseudo-code of our proposed evolutionary sampling strategy. Intuitively, Evo biases the sampling at every iteration to include more points from high PDE residual regions, Ω_{high} , and thus increase the representation of $\mathbb{E}_{\Omega_{high}}[\mathcal{L}_r(\theta)]$ in the overall PDE residual loss, in contrast to fixed sampling and dynamic random sampling. Also note that the computational complexity of Evo is same as the complexity of dynamic random sampling. Evo thus adds negligible computational overhead and does not slow down training in contrast to other sampling algorithms such as Monte Carlo sampling. See Appendix for detailed theoretical analysis and intuition behind the dynamics of Evolutionary Sampling algorithm.

4.2 Causal Extension of Evolutionary Sampling (Causal Evo)

In problems with time-dependent PDEs, a strong prior dictating the propagation of solution from initial points to interior points is the *principle of causality*, where the solution of the PDE at time t needs to be well-approximated before moving onto the solution at time $t + \Delta t$. To incorporate this prior guidance in our sampling framework, we present a Causal Extension of Evo (*Causal Evo*) that includes two modifications: (1) we develop a causal formulation of the PDE loss \mathcal{L}_r that pays attention to the temporal evolution of PDE solutions over training iterations, and (2) we develop a causally biased sampling scheme that additionally respects the causal structure while sampling collocation points. We describe both these modifications in the following.

Causal Formulation of PDE Loss. The key idea here is to utilize a simple time-dependent gate function $g(t)$ that can explicitly enforce causality by revealing only a portion of the entire time-domain to PINN training. Specifically, we introduce a continuous gate function $g(t) = (1 - \tanh(\alpha(\tilde{t} - \beta)))/2$, where β is the scalar shift parameter that controls the fraction of time that is revealed to the model, $\alpha = 5$ is a constant scalar parameter that determines the steepness of the gate, and \tilde{t} is the normalized time, i.e., $\tilde{t} = t/T$. Figure 5a shows example causal gates for different settings of β . We

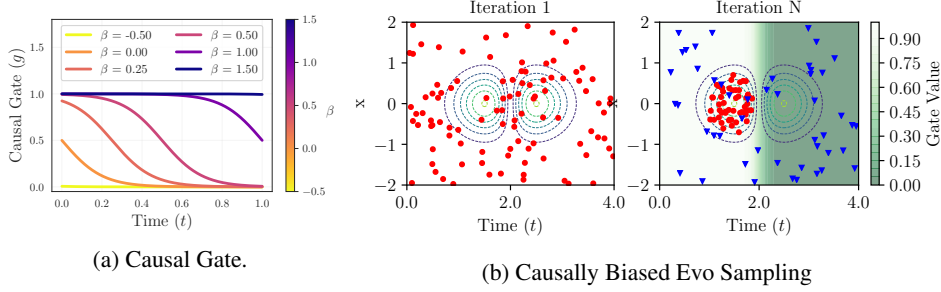


Figure 5: Causal Evo uses a time-dependent causal gate for computing PDE loss and for sampling.

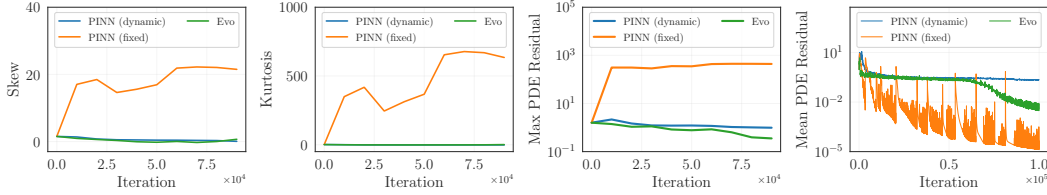


Figure 6: Comparison of Skewness, Kurtosis, Max PDE Residuals, and Mean PDE Residuals over training iterations for fixed vs. dynamic sampling methods for convection equation with $\beta = 50$.

use $g(t)$ to obtain a causally-weighted PDE residual loss as $\mathcal{L}_r^g(\theta) = \frac{1}{N_r} \sum_{i=1}^{N_r} [\mathcal{R}(x_r^i, t_r^i)]^2 * g(t_r^i)$. We initially start with a small value of the shift parameter ($\beta = -0.5$), which essentially only reveals a very small portion of the time domain as shown in Figure 5a, and then gradually increase β during training to reveal more portions of the time domain respecting the causal structure. For $\beta \geq 1.5$, the entire time domain is revealed, which is equivalent to the non-causal formulation.

Causally Biased Sampling. We bias the sampling strategy in Evo such that it not only favors the selection of collocation points from high residual regions but also accounts for the causal gate values at every iteration, as shown in Figure 5b. In particular, we simply modify the fitness function as $\mathcal{F}(\mathbf{x}_r) = |\mathcal{R}(\mathbf{x}_r)| * g(t_r)$ in the Evo algorithm, which biases the sampling to respect causality over iterations.

How to Update β ? To answer this question, we first examine the ideal behavior of the causal gate at some iteration i . At the next iteration, we should increase β_i to reveal a larger time domain *only if* the PDE residuals of collocation points at iteration i are low. Otherwise, β_i should remain in its place until the PDE residuals under the current gate is minimized. To achieve this behaviour, we propose the following update scheme for β : $\beta_{i+1} = \beta_i + \eta_g e^{-\epsilon \mathcal{L}_r^g(\theta)}$, where η_g is the learning rate that controls how fast the gate should propagate and ϵ denotes tolerance that controls how low the PDE loss needs to be before the gate shifts to the right. Since the update in β is inversely proportional to the causally-weighted PDE loss \mathcal{L}_r^g , the gate will shift slowly if the PDE residuals are large. Also note that increasing β also increases the value of $g(t)$ for all collocation points, thus increasing the causally-weighted PDE loss and slowing down gate movement. Upon convergence, β attains a large value such that the entire time domain is revealed.

5 Results

Table 1: Relative \mathcal{L}_2 errors of comparative methods over benchmark PDEs with $N_r = 1000$.

Equation	Max. Iters	PINN (fixed)	PINN (dynamic)	Curr. Reg.	cPINN (fixed)	cPINN (dynamic)	Evo (ours)	Causal Evo (ours)
Convection ($\beta = 30$)	100k	1.13E+00	2.03E-02	6.68E-01	1.45E+00	1.97E-02	1.26E-02	1.29E-02
	300k	1.14E+00	1.11E-02	2.07E-02	1.45E+00	1.08E-02	6.00E-03	5.21E-03
Convection ($\beta = 50$)	100k	1.02E+00	7.00E-01	9.13E-01	1.22E+00	1.24E+00	7.01E-02	4.39E-02
	300k	1.02E+00	5.93E-01	3.25E-01	1.19E+00	6.85E-01	1.86E-02	1.18E-02
Allen Cahn	200k	6.41E-01	8.28E-03	-	1.02E-01	3.01E-02	1.00E-02	7.12E-03

Experiment Setup. We perform experiments over three benchmark PDEs that have been used in the PINN literature to characterize the strengths and failure modes of PINNs. In particular, we consider

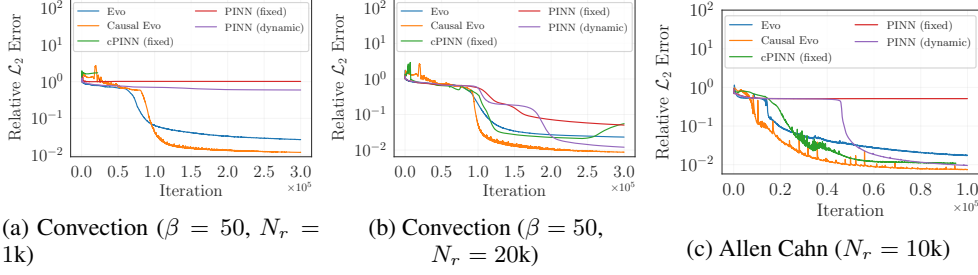


Figure 7: Comparing convergence speeds of baselines w.r.t. Evo and Causal Evo.

two time-dependent PDEs: convection equation (with $\beta = 30$ and $\beta = 50$) and Allen Cahn equation, and one time-independent PDE: the Eikonal equation for solving signed distance fields for varying input geometries. We consider the following baseline methods: (1) **PINN-fixed** (conventional PINN; using fixed sampling), (2) **PINN-dynamic** (using dynamic sampling), (3) **Curr. Reg.** (curriculum regularization method proposed in [6]), (4) **cPINN-fixed** (causal PINNs proposed in [17] with fixed sampling), and (5) **cPINN-dynamic** (cPINN with dynamic sampling). While comparing results for every benchmark PDE, we use the same neural network architecture and hyper-parameter settings across all baselines. We also use same architecture and hyper-parameter settings in our proposed methods, wherever possible. Details about the PDEs, experiment setups, and hyper-parameter settings are provided in the Appendix.

Effect of Dynamic Sampling. Figure 6 illustrates the value of dynamic sampling methods: PINN-dynamic and Evo, in mitigating the *propagation failure* mode of PINN-fixed, which is characterized by high Skewness, Kurtosis, and Max PDE residual values across iterations. We can see that even though the Mean PDE residual of PINN-fixed reduces over epochs, it is likely fitting to trivial solutions whose boundaries administer very high residuals in very narrow regions. On the other hand, PINN-dynamic and Evo are able to avoid the creation of imbalanced high residual regions and thus shows stable convergence w.r.t. the mean PDE loss. We also see that Evo shows a larger decline in the mean PDE loss after 50K iterations compared to PINN-dynamic while keeping skewness and Kurtosis low, indicating faster propagation of the correct solution from initial/boundary points. The evolution of collocation samples in Evo across training iterations is shown in the Appendix, where we show that the collocation points are getting accumulated in high PDE residual regions.

Comparing Prediction Performance. Table 1 shows the relative \mathcal{L}_2 errors of PDE solutions obtained by comparative methods w.r.t. ground-truth solutions for different time-dependent PDEs when N_r is set to 1K. We particularly chose a small value of N_r to study the effect of small sample size on PINN convergence (note that the original formulations of baseline methods used very high N_r). We can see that while PINN-fixed fails to converge for convection ($\beta = 30$) and Allen Cahn equations (admitting very high errors), PINN-dynamic shows significantly lower errors. This demonstrates the effectiveness of PINN-dynamic in mitigating propagation failures. However, for complex PDEs such as convection ($\beta = 50$), PINN-dynamic is still not able to converge to low errors. We also see that cPINN-fixed shows high errors across all PDEs when $N_r = 1000$. This is likely because the small size of collocation samples are insufficient for cPINNs to converge to the correct solution. As we show later, cPINN indeed is able to converge to the correct solution when N_r is large. Performing dynamic sampling with cPINN shows some reduction in errors, but it is still not sufficient for convection ($\beta = 50$) case. On the other hand, our proposed approaches (Evo and Causal Evo) consistently show the lowest errors across all PDEs.

Convergence Speed: Figure 7 shows that Causal Evo is able to converge faster to low error solutions than all other baseline methods for both convection and Allen Cahn equations. This shows the importance of respecting causality along with focusing on high residual regions to ensure

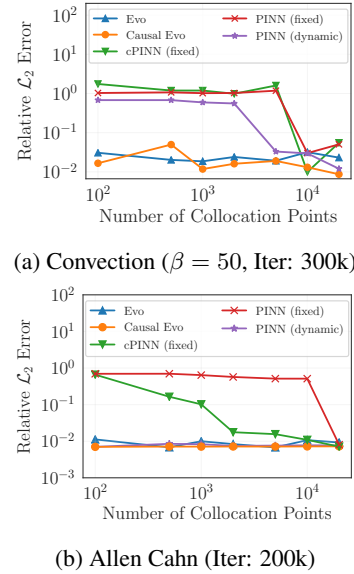


Figure 8: Sample Efficiency of Evo and Causal Evo at low N_r .

fast propagation of correct solution from initial/boundary points to interior points. While cPINN-fixed and PINN-dynamic do not converge for convection ($N_r = 1K$), we can see that they both converge to lower errors compared to PINN-fixed for Allen Cahn and for convection when N_r is large ($20K$).

Sampling Efficiency: Figure 8 shows the scalability of comparative methods to smaller sizes of sampled collocation points, N_r . Though all the baselines demonstrate similar performances when N_r is large ($> 10K$), only Evo and Causal Evo manage to maintain low errors even for very small values of $N_r = 100$, showing two orders of magnitude improvement in sampling efficiency. Note that the sample size N_r is directly related to the compute and memory requirements of training PINNs. Since Evo and Causal Evo can work in ultra-low sample size regimes, they are particularly useful for solving high-dimensional PDEs where sampling efficiency can greatly impact running time and memory consumption, e.g., in 3D fluid dynamics problems.

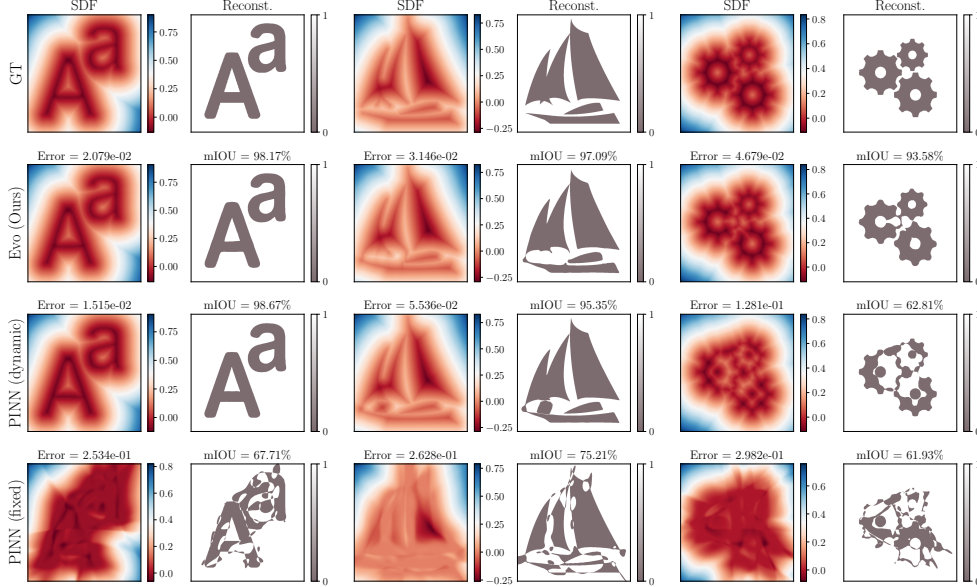


Figure 9: Solving Eikonal equation for signed distance field (SDF). The color of the heatmap represents the values of the SDF. The gray region shows the negative values of SDF that represents the interior points in the reconstructed geometry from predicted SDF.

Solving Eikonal Equations. Given the equation of a surface geometry in a 2D-space, $u(x_s, y_s) = 0$, the Eikonal equation is a time-independent PDE used to solve for the *signed distance field*(SDF), $u(x, y)$, which has negative values inside the surface and positive values outside the surface. See Appendix for details of the Eikonal equation.

We compare the performance of different baseline methods with respect to the ground-truth (GT) solution obtained from numerical methods for three complex surface geometries in Figure 9. The primary difficulty in solving Eikonal equation comes from determining the sign of the field (interior or exterior) in regions with rich details. We also plot the reconstructed geometry of the predicted solutions to demonstrate the real-world application of solving this PDE, e.g., in downstream real-time graphics rendering. The quality of reconstructed geometries are quantitatively evaluated using the mean Intersection-Over-Union (mIOU) metric that measures the degree of overlap between the predicted geometry and GT. The results show that PINN-fixed shows poor performance across all three geometries, while PINN-dynamic is able to capture most of the outline of the solutions with a few details missing for difficult geometries like “sailboat” and “gear”. On the other hand, Evo is able to capture even the fine details of the SDF for all three complex geometries and thus show better reconstruction quality. We can see that mIOU of Evo is significantly higher than baselines for “sailboat” and “gear”.

6 Conclusions And Future Work Directions

We present a novel perspective for identifying a failure modes in PINNs named “*propagation failure*” which are typically characterized by very narrow regions with high PDE residuals and demonstrate

that even a simple dynamic uniform sampling can help towards mitigating this. We further develop a novel *evolutionary sampling* algorithm where the collocation points dynamically evolve over the training iterations to prioritize high density regions to directly address the propagation failure mode. From our experiments, we demonstrate better performance, faster convergence as well as sample efficiency on benchmark PDEs. Future work can focus on theoretically understanding the interplay between minimizing PDE loss and sampling from high residual regions on PINN performance.

References

- [1] Jie Bu and Anuj Karpatne. Quadratic residual networks: A new class of neural networks for solving forward and inverse problems in physics involving pdes. In *Proceedings of the 2021 SIAM International Conference on Data Mining (SDM)*, pages 675–683. SIAM, 2021.
- [2] Agoston E Eiben, James E Smith, et al. *Introduction to evolutionary computing*, volume 53. Springer, 2003.
- [3] Ameya D Jagtap and George Em Karniadakis. Extended physics-informed neural networks (xpinn): A generalized space-time domain decomposition based deep learning framework for nonlinear partial differential equations. *Communications in Computational Physics*, 28(5): 2002–2041, 2020.
- [4] Ameya D Jagtap, Kenji Kawaguchi, and George Em Karniadakis. Adaptive activation functions accelerate convergence in deep and physics-informed neural networks. *Journal of Computational Physics*, 404:109136, 2020.
- [5] Stephen Kokoska and Daniel Zwillinger. *CRC standard probability and statistics tables and formulae*. Crc Press, 2000.
- [6] Aditi Krishnapriyan, Amir Gholami, Shandian Zhe, Robert Kirby, and Michael W Mahoney. Characterizing possible failure modes in physics-informed neural networks. *Advances in Neural Information Processing Systems*, 34, 2021.
- [7] Randall J LeVeque. *Finite difference methods for ordinary and partial differential equations: steady-state and time-dependent problems*. SIAM, 2007.
- [8] Levi McClenny and Ulisses Braga-Neto. Self-adaptive physics-informed neural networks using a soft attention mechanism. *arXiv preprint arXiv:2009.04544*, 2020.
- [9] Mohammad Amin Nabian, Rini Jasmine Gladstone, and Hadi Meidani. Efficient training of physics-informed neural networks via importance sampling. *Computer-Aided Civil and Infrastructure Engineering*, 36(8):962–977, 2021.
- [10] Maziar Raissi, Paris Perdikaris, and George Em Karniadakis. Physics informed deep learning (part i): Data-driven solutions of nonlinear partial differential equations. *arXiv preprint arXiv:1711.10561*, 2017.
- [11] Maziar Raissi, Paris Perdikaris, and George E Karniadakis. Physics-informed neural networks: A deep learning framework for solving forward and inverse problems involving nonlinear partial differential equations. *Journal of Computational Physics*, 378:686–707, 2019.
- [12] Robert E Schapire. The boosting approach to machine learning: An overview. *Nonlinear estimation and classification*, pages 149–171, 2003.
- [13] Alexander Shapiro. Monte carlo sampling methods. *Handbooks in operations research and management science*, 10:353–425, 2003.
- [14] Dan Simon. *Evolutionary optimization algorithms*. John Wiley & Sons, 2013.
- [15] Sifan Wang, Yujun Teng, and Paris Perdikaris. Understanding and mitigating gradient pathologies in physics-informed neural networks. *arXiv preprint arXiv:2001.04536*, 2020.
- [16] Sifan Wang, Hanwen Wang, and Paris Perdikaris. Learning the solution operator of parametric partial differential equations with physics-informed deepnets. *Science advances*, 7(40): eabi8605, 2021.

- [17] Sifan Wang, Shyam Sankaran, and Paris Perdikaris. Respecting causality is all you need for training physics-informed neural networks. *arXiv preprint arXiv:2203.07404*, 2022.
- [18] Sifan Wang, Xinling Yu, and Paris Perdikaris. When and why pinns fail to train: A neural tangent kernel perspective. *Journal of Computational Physics*, 449:110768, 2022.
- [19] Olek C Zienkiewicz, Robert L Taylor, and Jian Z Zhu. *The finite element method: its basis and fundamentals*. Elsevier, 2005.

A Additional Analysis of the Dynamics of Evolutionary Sampling

In this section, we analyze the dynamic behavior (or evolution) of the collocation points for our proposed *Evolutionary Sampling* (Evo) approach over the iterations.

A.1 Accumulation and Release of Collocation Points from High PDE Residual Regions.

We first describe how Evo is able to grow the representation of high PDE residual regions in the retained population at every iteration, thus helping to mitigate propagation failure modes in training PINNs. An underlying assumption of Evo is that the PDE residual field \mathcal{R} smoothly changes over consecutive iterations such that the retained points with high PDE residuals at a current iteration are representative of the high PDE residual regions of the next iteration. Further, some of the resampled points generated at the next iteration can also show high residual values, additionally increasing the coverage of high PDE residual regions at every iteration. Hence, if a high residual region persists for multiple iterations, more points would get accumulated in that region, increasing their contribution in the overall PDE residual loss and eventually resulting in their minimization. Once the PDE residuals in a certain region are resolved, the density of collocation points accumulated in that region would get released and used for re-sampling new points in the next iteration.

A.2 Preventing Sample Collapse.

From an optimization point of view, Evo aims to maximize the PDE residuals at the collocation points in the retained population at every iteration. However, a conventional (evolutionary) optimization algorithm would converge to a solution where every collocation point would collapse to a single point where the PDE residual is the highest (assuming that the PDE is constant during this optimization span). This “*sample collapse*” is detrimental from a sampling perspective in the training of PINNs as we are not interested in optimizing the PDE on a single point. Instead, we are interested in maintaining sufficient diversity in the collocation points to provide useful gradients of the PDE loss function in the training of PINNs and mitigate propagation failure modes. In the following, we describe how Evo ensures that the non-retained population (collection of collocation points with PDE residual values less than the threshold) converges to a uniform distribution and maintains sufficient diversity.

Let us denote the expectation of the fitness function (absolute value of the PDE residuals) for any general population \mathcal{P} be given as $\mathbb{E}[\mathcal{P}] = \mathbb{E}_{\mathbf{x}_r \in \mathcal{P}} [f(\mathbf{x}_r)]$. The expectation of fitness for the population generated by uniform sampling can then be defined as $\mathbb{E}[\mathcal{U}(\Omega)] = \mathbb{E}_{\mathbf{x}_r \sim \mathcal{U}(\Omega)} [f(\mathbf{x}_r)]$, while the expectation for the retained population at the i^{th} iteration can be defined as $\mathbb{E}[\mathcal{P}_i^r] = \mathbb{E}_{\mathbf{x}_r \in \mathcal{P}_i^r} [f(\mathbf{x}_r)]$. Let us denote $\overline{\mathcal{P}}_i^r$ as the complementary set of \mathcal{P}_i^r containing collocation points with fitness lower than or equal to threshold τ_i , i.e., $\overline{\mathcal{P}}_i^r \leftarrow \{\mathbf{x}_r^j : \mathcal{F}(\mathbf{x}_r^j) \leq \tau_i\}$. We refer to $\overline{\mathcal{P}}_i^r$ as the “non-retained” population. We can then define $\mathbb{E}[\mathcal{P}_i^s]$, $\mathbb{E}[\overline{\mathcal{P}}_i^r]$, and $\mathbb{E}[\mathcal{P}_i]$ as the expectation of fitness for the resampled population, non-retained population, and the entire population at iteration i , respectively. Note that the non-retained population is replaced by the resampled population at the next iteration, $i + 1$. The following theorem describes the stationary behavior of the non-retained population upon convergence, when there is no change in the expectation of fitness of the entire population over iterations.

Theorem 1 *The expectation of fitness of the non-retained population converges to the steady state of $\mathbb{E}[\overline{\mathcal{P}}_i^r] = \mathbb{E}[\mathcal{U}(\Omega)]$ when $\mathbb{E}[\mathcal{P}_i]$ converges to a constant value over iterations.*

Proof. Since we are using the mean of the PDE residuals of population \mathcal{P}_i as the threshold $\tau_i = \mathbb{E}[\mathcal{P}_i]$, the retained and resampled populations cannot be empty. Also, since the fitness of every collocation point in \mathcal{P}_i is greater than τ_i , by definition, $\mathbb{E}[\mathcal{P}_i^r] > \mathbb{E}[\mathcal{P}_i]$. Also, since the resampled population is generated from a uniform distribution, we know that $\mathbb{E}[\mathcal{P}_i^s] = \mathbb{E}[\mathcal{U}(\Omega)]$. The expectation of the fitness of the population at the $(i + 1)^{th}$ epoch can then be written as:

$$\begin{aligned} \mathbb{E}[\mathcal{P}_{i+1}] &= \mathbb{E}[\mathcal{P}_i^r \cup \mathcal{P}_i^s] = k_{i+1} \mathbb{E}[\mathcal{P}_i^r] + (1 - k_{i+1}) \mathbb{E}[\mathcal{P}_i^s], \\ &= k_{i+1} \mathbb{E}[\mathcal{P}_i^r] + (1 - k_{i+1}) \mathbb{E}[\mathcal{U}(\Omega)]. \end{aligned} \quad (4)$$

Here, k_i is a constant and is equal to $|\mathcal{P}_i^r| / (|\mathcal{P}_i^r| + |\mathcal{P}_i^s|)$, where $|\mathcal{P}|$ denotes the number of points in an arbitrary population \mathcal{P} . Similarly, we can write the expectation of fitness of the population at

iteration i as:

$$\mathbb{E}[\mathcal{P}_i] = \mathbb{E}[\mathcal{P}_i^r \cup \overline{\mathcal{P}_i^r}] = k_i \mathbb{E}[\mathcal{P}_i^r] + (1 - k_i) \mathbb{E}[\overline{\mathcal{P}_i^r}], \quad (5)$$

where k_i is a constant and is equal to $|\mathcal{P}_i^r|/(|\mathcal{P}_i^r| + |\overline{\mathcal{P}_i^r}|)$. Since $|\overline{\mathcal{P}_i^r}| = |\mathcal{P}_i^s|$, $k_i = k_{i+1}$.

Hence, from Equations 4 and 5, we can say that $\mathbb{E}[\mathcal{P}_{i+1}] > \mathbb{E}[\mathcal{P}_i]$ (i.e., there is an increase in expectation of fitness of the population going from iteration i to $i + 1$) when $\mathbb{E}[\mathcal{P}_i^r] < \mathbb{E}[\mathcal{U}(\Omega)]$. On the other hand, when $\mathbb{E}[\mathcal{P}_i^r] \geq \mathbb{E}[\mathcal{U}(\Omega)]$, the expectation of fitness of the population would decrease as we go from iteration i to $i + 1$, i.e., $\mathbb{E}[\mathcal{P}_{i+1}] \leq \mathbb{E}[\mathcal{P}_i]$. Hence, depending on whether the expectation of fitness of the non-retained population is greater than or lesser than that of uniform distribution, the expectation of fitness of the entire population would keep on fluctuating. Upon convergence, we expect $\mathbb{E}[\mathcal{P}_{i+1}] = \mathbb{E}[\mathcal{P}_i]$, i.e., the expectation of fitness of the entire population will remain constant. This is only possible when the non-retained population converges to the stationary state where $\mathbb{E}[\overline{\mathcal{P}_i^r}] = \mathbb{E}[\mathcal{U}(\Omega)]$. Therefore, evolutionary sampling will not lead to unconstrained growth of the expectation of fitness that may increase the risk of entire population converging into a small region, which is different from conventional optimization settings where the goal is to simply maximize the expectation of population fitness. Instead, upon convergence, we see that the non-retained population of Evo will have an expectation that is same as that of points sampled from the uniform distribution, ensuring sufficient diversity of points.

B Additional Details for Causal Evolutionary Sampling

B.1 Preventing Abrupt Causal Gate Movement.

The shift parameter β of the causal gate is updated every iteration using the following scheme: $\beta_{i+1} = \beta_i + \eta_g e^{-\epsilon \mathcal{L}_r^g(\theta)}$, where η_g is the learning rate that controls how fast the gate should propagate and ϵ denotes tolerance that controls how low the PDE loss needs to be before the gate shifts to the right, and i denotes the i^{th} iteration. Typically, in our experiments we set the learning rate to 1e-3. Thus, for example, if the expectation of $e^{-\epsilon \mathcal{L}_r^g(\theta)}$ over 1000 iterations is 0.1, then β would change by a value of 0.1 after 1000 iterations (since $\beta_{i+N} \approx \beta_i + \eta_g * N * \mathbb{E}[e^{-\epsilon \mathcal{L}_r^g(\theta)}]$). Additionally, note that, for a typical ‘‘tanh’’ causal gate, the operating range of β values vary from -0.5 to 1.5 . However, if the loss is very small ($\mathcal{L}_r^g(\theta) \rightarrow 0$), the magnitude of the update $e^{-\epsilon \mathcal{L}_r^g(\theta)} \rightarrow 1$, i.e., leads to an abrupt change in the causal gate. Thus, to prevent an abrupt gate movement due to large magnitude update, we employ a magnitude clipping scheme (similar to gradient clipping in conventional ML) as follows: $\beta_{i+1} = \beta_i + \eta_g \min(e^{-\epsilon \mathcal{L}_r^g(\theta)}, \Delta_{max})$, where Δ_{max} is the maximum allowed magnitude of update. Typically, for our experiments we keep $\Delta_{max} = 0.1$. Note, that Δ_{max} needs to be carefully chosen depending on the gate learning rate η_g .

B.2 Choice of Other Gate Functions.

The gate function g to enforce the principle of causality is not limited to the ‘‘tanh’’ gate presented in Section 4.2 of the main paper. Any arbitrary function can be used for a causal gate as long as it obeys the following criteria:

1. **Continuous Time Property:** The function g should be continuous in time, such that it can be evaluated at any arbitrary time t .
2. **Monotonic Property:** The value of gate g at time $t + \Delta t$ should be less than the value of the gate at time t , i.e., $g(t + \Delta t) \leq g(t)$. In other words, g should be a monotonically decreasing function,
3. **Shift Property:** The gate function should be parameterized using a shift parameter β , such that $g_\beta(t) < g_{\beta+\delta}(t)$, where $\delta > 0$, i.e., by increasing the value of the shift parameter the gate value of any arbitrary time should increase.

An alternate choice of a causal gate is using a composition of ReLU and tanh functions: $g = \text{ReLU}(-\tanh(\alpha(t - \beta)))$ (as shown in Figure 10). We can see that by using ReLU, this alternate gate function provides a stricter thresholding of gate values to 0 after a cutoff value of time. The effect of this strict thresholding on the incorporation of causality in training PINNs can be studied in future analyses. In our current analysis, we simply used the tanh gate function for all our experiments.

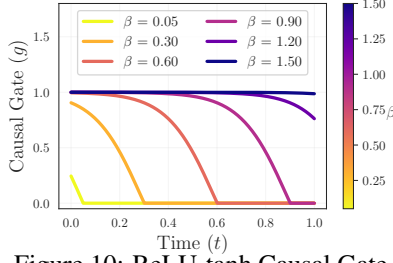


Figure 10: ReLU-tanh Causal Gate

C Details of Partial Differential Equations Used in the Paper

C.1 Convection Equation

We considered a 1D-convection equation that is commonly used to model transport phenomenon, described as follows:

$$\frac{\partial u}{\partial t} + \beta \frac{\partial u}{\partial x} = 0, \quad x \in [0, 2\pi], t \in [0, 1] \quad (6)$$

$$u(x, 0) = h(x) \quad (7)$$

$$u(0, t) = u(2\pi, t) \quad (8)$$

where β is the convection coefficient and $h(x)$ is the initial condition. For our case studies, we used a constant setting of $h(x) = \sin(x)$ with periodic boundary conditions in all our experiments, while varying the value of β in different case studies.

C.2 Allen-Cahn Equation

We considered a 1D - Allen Cahn equation that is used to describe the process of phase-separation in multi-component alloy systems as follows:

$$\frac{\partial u}{\partial t} - 0.0001 \frac{\partial^2 u}{\partial x^2} + 5u^3 - 5u = 0, \quad x \in [-1, 1], t \in [0, 1] \quad (9)$$

$$u(x, 0) = x^2 \cos(\pi x) \quad (10)$$

$$u(t, -1) = u(t, 1) \quad (11)$$

$$\frac{\partial u}{\partial t} \Big|_{x=-1} = \frac{\partial u}{\partial t} \Big|_{x=1} \quad (12)$$

C.3 Eikonal Equation

We formulate the Eikonal equation for signed distance function (SDF) calculation as:

$$|\nabla u| = 1, \quad x, t \in [-1, 1] \quad (13)$$

$$u(x_s) = 0, \quad x_s \in \mathcal{S} \quad (14)$$

$$u(x, -1), u(x, 1), u(-1, y), u(1, y) > 0 \quad (15)$$

where \mathcal{S} is zero contour set of the SDF. In training PINN, we use the zero contour constraint as initial condition loss and positive boundary constraint as boundary loss (see Table 2 for details of loss balancing).

D Details on Skewness and Kurtosis Metrics

Skewness and kurtosis are two basic metrics used in statistics to characterize the properties of a distribution of values $\{Y_i\}_{i=1}^N$. A high value of Skewness indicates lack of symmetry in the

distribution, i.e., the distribution of values to the left and to the right of the center point of the distribution are not identical. On the other hand, a high value of Kurtosis indicates the presence of a heavy-tail, i.e., there are more values farther away from the center of the distribution relative to a Normal distribution. In our implementation using *scipy*, we used the adjusted Fisher-Pearson coefficient of skewness and Fisher’s definition of kurtosis, as defined below.

Skewness: For univariate data Y_1, Y_2, \dots, Y_N , the formula of skewness is

$$\text{skewness} = \frac{\sqrt{N(N-1)}}{N-2} \times \frac{\sum_{i=1}^N (Y_i - \bar{Y})^3 / N}{s^3}, \quad (16)$$

where \bar{Y} is the sample mean of the distribution and s is the standard deviation. For any symmetric distribution (e.g., Normal distribution), the skewness is equal to zero. A positive value of skewness means there are more points to the right of the center point of the distribution than there are to the left. Similarly, a negative value of skewness means there are more points to the left of the center point than there are to the right. In our use-case, a large positive value of skewness of the PDE residuals indicates that there are some asymmetrically high PDE residual values to the right.

Kurtosis: Kurtosis is the fourth central moment divided by the square of the variance after subtracting 3, defined as follows:

$$\text{kurtosis} = \frac{\sum_{i=1}^N (Y_i - \bar{Y})^4 / N}{s^4} - 3 \quad (17)$$

For a Normal distribution, Kurtosis is equal to 0. A positive value of Kurtosis indicates that there are more values in the tails of the distribution than what is expected from a Normal distribution. On the other hand, a negative value of Kurtosis indicates that there are lesser values in the tails of the distribution relative to a Normal distribution. In our use-case, a large positive value of Kurtosis of the PDE residuals indicates that there are some high PDE residual values occurring in very narrow regions of the spatio-temporal domain, that are being picked up as the heavy-tails of the distribution.

E Hyper-parameter Settings and Implementation Details

The hyper-parameter settings for the different baseline methods for every benchmark PDE are provided in Table 2. Note that we used the same network architecture and other hyper-parameter settings across all baseline method implementations for the same PDE. In this table, the column on ‘r/ic/bc’ represents the setting of the $\lambda_r, \lambda_{ic}, \lambda_{bc}$ hyper-parameters that are used to weight the different loss terms in the overall learning objective of PINNs. Table 2 also lists the type of Optimizer, learning rate (lr), and learning rate scheduler (lr.scheduler) used across all baselines for every PDE. For the Eikonal equation, we used the same modified multi-layer perceptron (MLP) architecture as the one proposed in [15]. Additionally, for the Causal Evolutionary Sampling method, we used the following hyper-parameter settings across all PDEs: $\alpha = 5$, learning rate of the gate $\eta_g = 1e-3$, tolerance $\epsilon = 20$, initial value of $\beta = -0.5$, and $\Delta_{max} = 0.1$. The number of iterations (and the corresponding PDE coefficients for the Convection Equation) are provided in Section 5 of the main paper.

Hardware Implementation Details: We trained each of our models on one Nvidia Titan RTX 24GB GPU.

F Additional Visualizations

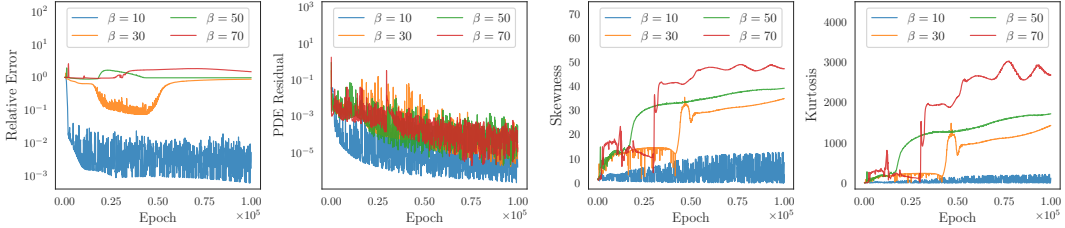
F.1 Visualizing Propagation Failure for Different Settings of β

In Figure 2 of the main paper, we demonstrated the phenomenon of propagation failure for convection equation with $\beta = 50$, which was characterized by large values of Skewness and Kurtosis in the PDE residual fields for a large number of iterations (or epochs), and a simultaneous stagnation in the relative error values even though the mean PDE residual kept on decreasing. Here, in Figure 11, we show that the same phenomenon can be observed for other large values of $\beta > 10$, namely, $\beta = 30, 50, 70$. We can see that the relative errors for all these three cases remains high even though the PDE residual loss keeps on decreasing with iterations. We can also see that the absolute values

Table 2: Hyper-parameter settings for different baseline methods for every benchmark PDE

PDE	Method	Architecture	Periodic Encoding	r/ic/bc	Optimizer/ lr	lr. scheduler
Convection	PINN, cPINN, Evo, CausalEvo	50×4 (MLP)	No	1/100/100	Adam/ 1e-3	StepLR rate=0.9 steps=5000
	Curr. Reg.	50×4 (MLP)	No	1/1/1	Adam/ 1e-4	No
Allen Cahn	PINN, cPINN, Evo, CausalEvo	128×4 (MLP)	Yes	1/100/-	Adam/ 1e-3	StepLR rate=0.9 steps=5000
Eikonal	PINN, Evo	128×4 (modified MLP) [15]	No	1/500/10	Adam/ 1e-3	StepLR rate=0.9 steps=5000

of skewness and kurtosis increase as we increase β , indicating higher risks of propagation failure. In fact, for $\beta = 30$, we can even see that the epoch that marks an abrupt increase in skewness and kurtosis (around 50K iterations) also shows a sudden increase in the relative error at the same epoch, highlighting the connection between imbalanced PDE residuals and the phenomenon of propagation failure.

Figure 11: Demonstration of Propagation Failure for Different Settings of β ($\beta = 10, 30, 50, 70$)

F.2 Visualizing the Evolution of Collocation Points in Evo

Figure 12 shows the evolution of collocation points and PDE residual maps of Evo as we progress in training iterations for the convection equation with $\beta = 50$. We can see that the retained population of Evo at every iteration (shown in red) selectively focuses on high PDE residual regions, while the re-sampled population (shown in blue) are generated from a uniform distribution. By increasing the contribution of high residual regions in the computation of the PDE loss, we can see that Evo is able to reduce the PDE loss over iterations without admitting high imbalance, thus mitigating the propagation failure mode, in contrast to conventional PINNs.

F.3 Visualizing the Evolution of Collocation Points in Causal Evo

Figure 13 shows the evolution of collocation points and PDE residuals of Causal Evo, along with the dynamics of the Causal Gate function. We can see that the retained population at every iteration (shown in red) strictly adheres to the principle of causality such that the collocation points are sampled from later times only when the PDE residuals at earlier times have been minimized. This is also reflected in the movement of the causal gate function where the gate values are close to 1 for only small portions of time domain at intermediate epochs. At 90K iterations, we can see that the causal gate values are close to 1 for all values of time, indicating that the entire time domain is now revealed for training PINN to converge to the correct solution.

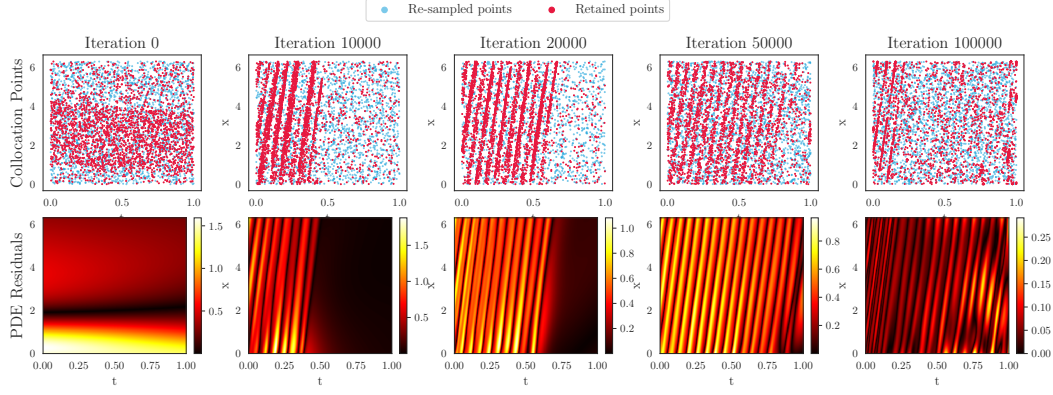


Figure 12: Evolution of collocation points of Evo for convection equation with $\beta = 50$.

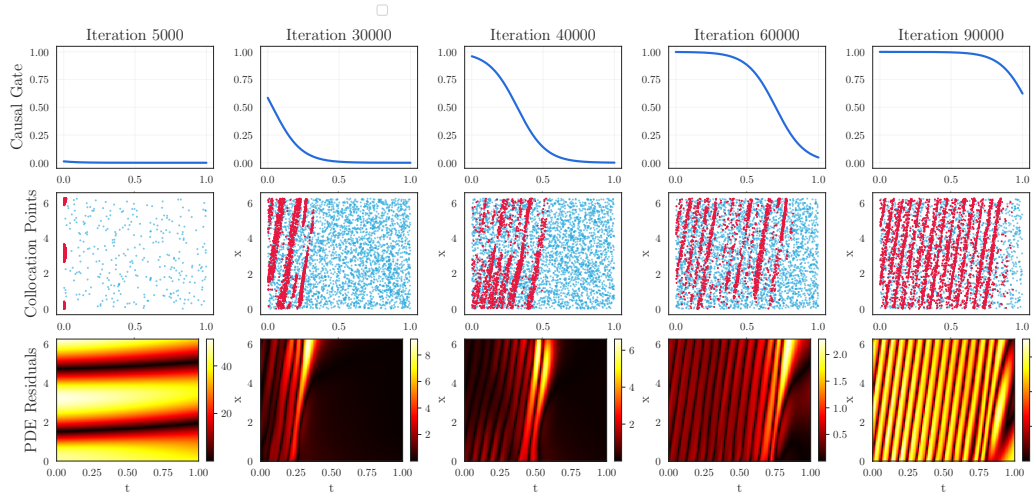


Figure 13: Evolution of collocation points of Causal Evo for convection equation with $\beta = 50$.